Vision-Based Active Sensor Using a Flexible Beam

Makoto Kaneko, *Senior Member, IEEE*, Naoki Kanayama, and Toshio Tsuji, *Member, IEEE*

***Abstract*—This paper proposes a new vision-based active sensing system, termed vision-based active antenna. This is composed of a camera, a flexible beam whose force-deformation characteristic is known, and an actuator for rotating the beam. The camera observes the beam deformation, including the contact information, while the beam is in contact with an object. By solving a set of equations based on the information acquired through the camera, the sensor can detect the contact location, the contact force, and the stiffness of the object, even though the contact point is hidden by occlusion. For two particular versions, we show some experimental results to verify the basic idea.**

***Index Terms*—Contact force, contact point, stiffenss sensing, tactile sensor.**

I. Introduction

THE human sense of touch provides us with an important source of information about our surroundings. Because of its unique position as the interface between our bodies and the outside world, touch sensing supplies sensory data that help us to manipulate and to recognize objects and be warned of harmful situations. Many creatures, including humans, make good use of the tactile information they obtain through physical contact with external objects. Tactile sensing is very direct. It is not distorted by perspective, confused by external lighting, or greatly affected by the material constitution or surface finish of objects. We humans use tactile information to maintain the posture of our bodies, to provide a warning of physical danger, and to monitor walking and grasping. Tactile sensing has the potential to fill a similar sensing role for robotics systems.

So far, a number of tactile sensors have been proposed [1]–[11] and implemented in various robotic systems, especially grippers and multifingered robot hands. The use of tactile sensors for either recognizing the shape of an object [7]–[9] or detecting the local contact point between the sensor and an object [10], [11] has been discussed in the literature. Most previous works implicitly assume that the tactile sensor is already placed close to the target object and ready to start a sensing action. In general cases, however, a robot has to begin by finding the target object itself, before starting any tactile motion. Fig. 1(a) shows a sensing procedure for such a case, where the mobile robot is equipped with a tactile sensor only and no other external sensors. S_1 and S_2 denote the starting points for finding the target object and for obtaining the tactile information, respectively. The sensing procedure is classified into two phases, namely, the approach phase, where the robot approaches the target object, and the detection phase, where the robot detects the shape of an object by moving the tactile sensor. As seen from Fig. 1(a), this sensing procedure, especially in the approach phase, is particularly inefficient since the robot has to repeat side-and-forward motions until it reaches the target object. On the other hand, suppose that the robot is equipped with a vision sensor, as shown in Fig. 1(b). In such a case, the robot will be able to immediately recognize the rough position of object. Once the robot knows roughly an object's position, it can quickly reach the starting position S_2. The same situation will apply even if we replace a mobile robot with a manipulator. Through these examples, we can see that a sensor such as vision helps greatly in guiding the robot to the target object since it can obtain global information of environment. After such an approach phase, the tactile sensor can take responsibility. Thus, visual assistance during the approach phase is especially important when the robot obtains the surface profile of an object through touch in an unstructured environment. Based on this consideration, we assume that a vision sensor is already implemented to assist tactile sensing.

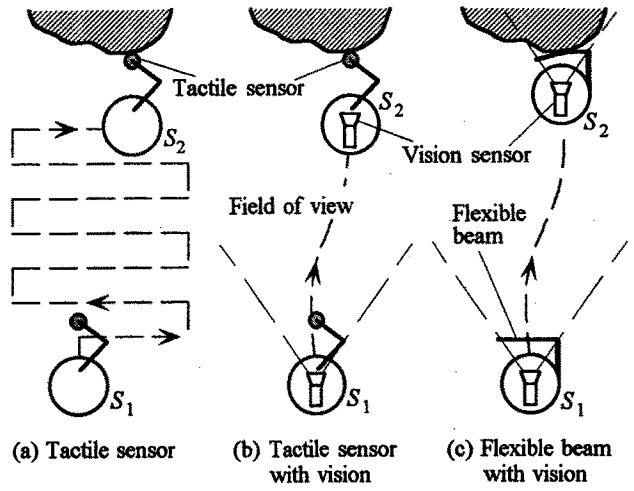

Fig. 1. Environment sensing by a tactile sensor and a vision sensor.

In this paper, we will discuss a new vision-based active sensor, where a vision system is used for the detection phase as well as the approach phase. For the detection phase, the vision observes the deformation of a flexible beam, as shown in Fig. 1(c). When a flexible beam with a straight line is in contact with an object, it is deformed according to how much force is applied and where it makes contact. The beam keeps a straight line after the contact point, while it is deformed into a

Manuscript received February 18, 1999; revised April 3, 2000. This work was supported in part by the Ministry of Education, Japan, under Grant-in-Aid for Scientific Research 08 650 316. Recommended by Technical Editor T. J. Tarn.

M. Kaneko and T. Tsuji are with the Faculty of Engineering, Hiroshima University, Higashi-Hiroshima 739-8527, Japan (e-mail: kaneko@huis.hiroshima-u.ac.jp).

N. Kanayama was with the Faculty of Engineering, Hiroshima University, Higashi-Hiroshima 739-8527, Japan. He is now with Harmonic Drive Systems, Co. Ltd., Japan (e-mail: n.kanayama@hds.co.jp).

Publisher Item Identifier S 1083-4435(01)02722-3.

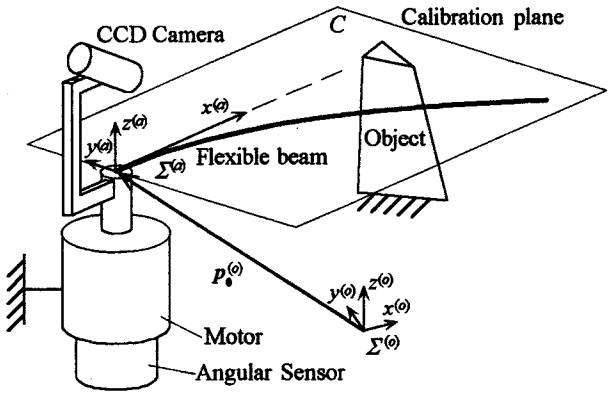

Fig. 2. An overview of the vision-based active antenna.

curved line between the base and the contact point. This means that the beam shape in contact with an object contains contact information, such as contact point, contact force, and perhaps local stiffness of an object.

With this information in mind, we will propose a new active sensing system called vision-based active antenna (VBAA), composed of one flexible beam, one actuator to rotate the beam, one position sensor to measure the rotation angle of the beam, and one charge-coupled device (CCD) camera to observe the beam's shape, as shown in Fig. 2. The actuator can be replaced either by driving wheels in a mobile robot or by joint actuators in a robot manipulator. Hereafter, we focus on the detection phase only. An active motion is imparted to the beam while it is in contact with the object. The camera continuously observes the beam's shape. By observing the shape distortion from its original straight-line position, the sensor system can detect any initial contact with the object. With a further active motion, the beam deforms according to the pushing angle, the contact location, and the object's stiffness. The pushing angle after contact can be regarded as input for the VBAA, and the beam's shape obtained through the CCD camera can be regarded as output. From the input–output relationship, we obtain a set of equations, which in turn include the contact information. By solving these equations, the VBAA can detect the contact distance, the contact force, and the object's stiffness. It is interesting to note that the VBAA can work even under occlusion where the contact point is hidden. Our experiments show that the VBAA provides highly accurate contact information, even under conditions where up to 65% of the beam is hidden by occlusion.

This paper is organized as follows. We will begin by explaining the basic structure and assumptions of the VBAA in Section III. In Section V, we will describe the basic working principle of the VBAA. We will also show several experimental results to verify the basic idea in Section VI. We will conclude in Section VIII, after some discussions on application and accuracy in Section VII.

II. Related Works

A simple flexible beam sensor can take the form of a short length of spring piano wire or hypodermic tubing anchored at the end. When the free end touches an external object, the wire bends. This can be sensed by a piezoelectric element or by a simple switch [10]. A more elaborate sensor is described by Wang and Will [11]. Long antenna-like whisker sensors were mounted on the SRI mobile robot, Shakey [12], and on Brook's six-legged robot insects [13]. Hirose *et al.* discussed the utilization of whisker sensors in legged robots [14]. The sensor system is composed of an electrode and a whisker whose end is fixed at the base. This sensor unit has been arranged in an array around each foot of the legged robot, Titan III, so that it can monitor the separation between each foot and the ground to allow for deceleration of the foot before contact. This sensor is also conveniently used to confirm which part of the foot is in contact with the ground. Similarly shaped whiskers have been considered for the legs of The Ohio State University's active suspension vehicle [15]. Russell developed a sensor array [16] by mounting whisker sensors on a mobile robot and succeeded in reconstructing the shape of a convex object. In his work, it is assumed that the whisker tip is always in contact with the object, and that when any part of a whisker other than the tip comes into contact with the object, it is assigned as a failure. Ueno *et al.* [17] proposed the basic concept on dynamic contact sensing by using a flexible beam, where it can estimate the contact location through the natural frequency observed while the beam is in contact with an object. The major difference between previous works [10]–[17] and ours is that the VBAA can detect not only a contact point between the antenna and the object but also the object's stiffness and contact force.

There are several works combining both tactile and visual sensors to take advantage of each sensor. For example, Stansfield presented a robotic perceptual system that utilizes passive vision and active touch [18]. Allen proposed an object-recognition system that uses passive stereo vision and active exploratory tactile sensing [19]. Vischer designed and developed a cooperating robot with vision and tactile sensors [20]. Sakane *et al.* presented an approach to estimate a contact point between a grasped object and an environment by utilizing vision and force sensors [21]. Nelson and Khosla utilized both force and vision for improving manipulator impact response [22]. All of these works utilized two different kinds of sensors to increase sensing ability.

In these works, the tactile sensor is most often utilized for obtaining the shape of an object in a particular area where a vision sensor does not provide any meaningful information due to factors such as occlusion, or insufficient illumination, whereas the VBAA can provide contact information even without any tactile sensor, and even under occlusion.

III. Basic Structure and Assumptions

A. Basic Structure

Fig. 2 shows an overview of the VBAA, where $\Sigma^{(a)}$ and $\Sigma^{(o)}$ are the antenna and the world coordinate systems, respectively. This system has one motor to rotate a beam and one CCD camera mounted on the joint. The CCD camera is not for observing the contact point directly but for obtaining the shape of the deformed beam.

In practice, there are two choices for implementing a CCD camera, namely, to mount it on the fixed coordinate system or on

the moving coordinate system, as shown in Fig. 2. An advantage of mounting it on the fixed coordinate system is that we can remove the angular sensor for measuring the position of the beam, since a CCD camera can detect the position of the beam by itself. However, the resolution for measuring the beam's shape will be lessened by the use of a lens with a wide enough viewing angle to cover the whole working area of the beam. In the approach mounting a CCD on the coordinate system rotating with the output shaft of the actuator, we can relatively increase the resolution for measuring the beam's shape, since we can focus on the limited viewing area where the beam can be observed. In order to obtain the basic characteristics such as accuracy, resolution, and sensitivity, we adopted the latter mode for implementing the CCD camera in the VBAA system, even though it needs a joint position sensor for determining the absolute position of the beam.

B. Main Assumptions

Our main assumptions are as follows.

Assumption 1) The deformation of beam is small enough to ensure that the beam's behavior obeys the force-deformation relationship based on linear theory.

Assumption 2) The object does not move during active motions.

Assumption 3) The elongation of beam due to unit axial force is negligibly small compared with the deflection due to a unit bending force.

Assumption 4) The beam is connected to the actuator shaft at the center of rotation.

Assumption 5) The cross section of the elastic beam is circular and the radius is constant along the longitudinal axis.

Assumption 6) Point contact is maintained between the object and the beam.

As the deformation of a beam increases, the relationship between the contact force and the deformation gradually moves away from a linear one and shows nonlinear behavior. Assumption 1) is for avoiding such nonlinear behavior between the two, which is important if we are to ensure the uniqueness of solution. Assumption 3) implies that the beam is very stiff in its axial direction, while it is relatively compliant in nonaxial direction. To simplify the discussions, we neglect the effect of an adapter with Assumption 4). For practical application, however, the sensing system needs a proper adaptor for connecting an actuator with the beam, and such an adaptor has high stiffness when compared with the beam. With Assumption 5), we can expect an equal compliance in the plane perpendicular to the longitudinal axis. This means that both directions of contact force and the deformation vectors are the same as each other. Under Assumption 5), it is guaranteed that the deformed beam lies on the plane where the contact force exists. Assumption 6) is important for guaranteeing the uniqueness of solution when obtaining the contact point from two measured points.

C. Importance of the Beam Elasticity

Now, suppose a rigid beam with scaling. For the contact point detection, the CCD camera will be able to directly read the scale in contact with the object, if a good working condition is prepared for visual sensing. However, because of occlusion or lighting problems, providing good conditions for a vision system is not always easy, and the real contact point is often hidden or unreadable in an ambiguous scene. When the beam makes contact with a compliant object, it is particularly difficult to find an exact contact point since it sinks into the surface. Furthermore, a rigid beam produces an impulsive force when it collides with an object at speed. Thus, the VBAA using a rigid beam does not seem to work successfully in a practical environment. Let us now assume that the beam is elastic and that its force-deformation behavior is known in advance. When such a beam makes contact with an object, it deforms according to the contact point, the pushing angle, and the object's stiffness. The beam deforms between the base and the contact point, while the remaining part of the beam remains in a straight line. By utilizing this information, the VBAA can evaluate the contact point. Later, we will show that two arbitrary points on the beam are both necessary and sufficient for determining the beam's unique shape, if the deformation plane is given. In other words, if the sensor system can measure two points on the beam, the unique contact point is obtained. This is the great advantage in utilizing a flexible beam, since the sensor system can provide the contact point without requiring any information concerning the exact contact point.

IV. Geometrical Expressions

A. Relationship Between Antenna and World Coordinates

Let $\mathbf{p}^{(a)}$ be the vector pointing to a position on the antenna. The transformation from the antenna to the world coordinate system is given by

$$\mathbf{p}^{(o)} = \mathbf{p}_0^{(o)} + \mathbf{R}_a^o \mathbf{p}^{(a)} \tag{1}$$

$$\mathbf{p}^{(a)} = \left(x^{(a)}, y^{(a)}, z^{(a)}\right)^T \tag{2}$$

$$\mathbf{p}_0^{(o)} = \left(x_0^{(o)}, y_0^{(o)}, z_0^{(o)}\right)^T \tag{3}$$

$$\mathbf{R}_a^o = \begin{bmatrix} \cos\phi & -\sin\phi & 0 \\ \sin\phi & \cos\phi & 0 \\ 0 & 0 & 1 \end{bmatrix} \tag{4}$$

where $\mathbf{p}_0^{(o)}$, ϕ and $\mathbf{R}_a^o$ denote the position vector between the origins of two coordinate systems and the angle for the motor and the rotational matrix from $\Sigma^{(a)}$ to $\Sigma^{(o)}$, respectively. Hereafter, we focus on the position sensing on the antenna coordinate system.

B. Relationship Between Deformation Plane and Observing Point

We define the deformation plane $\mathcal{D}$ and the calibration plane $\mathcal{C}$ as shown in Fig. 3, where ψ denotes the inclination angle of the deformation plane with respect to the calibration plane. For our simplicity, the calibration plane $\mathcal{C}$ is so chosen that it may coincide with the $x^{(a)}y^{(a)}$ plane in the antenna coordinate system $\Sigma^{(a)}$. The calibration of the CCD camera is done on $\mathcal{C}$ by using a network line whose scale is known. Therefore, the

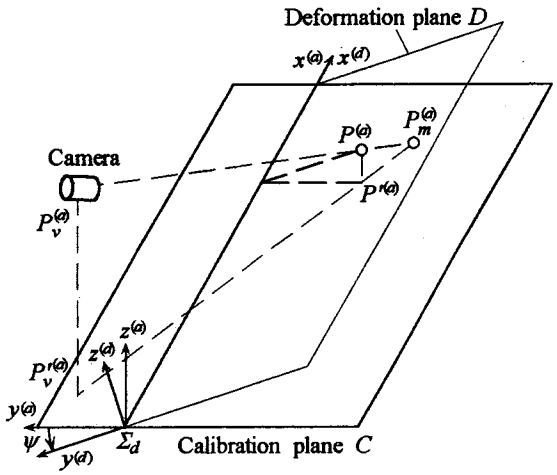

Fig. 3. A point projected on the calibration plane $\mathcal{C}$.

camera can detect points over the beam projected on $\mathcal{C}$ through the vision system. Now, suppose that a cubic object is placed perpendicular to the plane where the beam is rotating. For such an object, the contact point on the object does not change after a pushing motion. This means that the whole beam still lies on the calibration plane $\mathcal{C}$ even after deformation. Now, suppose we have an object as shown in Fig. 2. For such an object, the beam will move up along the edge during the increase of rotating angle of the motor. In other words, the beam no longer exists on the calibration plane $\mathcal{C}$ but lies on the particular plane under Assumption 5). This is what we call the *deformation plane* $\mathcal{D}$. We assign the deformation coordinate system $\Sigma^{(d)}$ for $\mathcal{D}$, where $\mathcal{D}$ corresponds to the $x^{(d)}y^{(d)}$ plane in $z^{(d)} = 0$. We note that the force-deformation relationship exists on $\mathcal{D}$, while the CCD camera can detect points on the beam projected on $\mathcal{C}$.

A point $(x^{(d)}, y^{(d)}, 0)$ in the deformation coordinate system is transformed into the antenna coordinate system by the following relationship:

$$\begin{pmatrix} x^{(a)} \\ y^{(a)} \\ z^{(a)} \end{pmatrix} = \begin{pmatrix} x^{(d)} \\ y^{(d)} \cos\psi \\ y^{(d)} \sin\psi \end{pmatrix}. \tag{5}$$

Suppose that a point $(x^{(a)}, y^{(a)}, z^{(a)})$ on the antenna is transformed by $(x_m^{(a)}, y_m^{(a)}, 0)$ on $\mathcal{C}$. Under such a condition, $\triangle P_m^{(a)} P_v^{(a)} P_v'^{(a)}$ and $\triangle P_m^{(a)} P'^{(a)} P^{(a)}$ become similar to each other, as shown in Fig. 3. This similarity relationship is given by

$$\begin{pmatrix} x_m^{(a)} - x^{(a)} \\ y_m^{(a)} - y^{(a)} \end{pmatrix} = \frac{z^{(a)}}{z_v^{(a)}} \begin{pmatrix} x_m^{(a)} - x_v^{(a)} \\ y_m^{(a)} - y_v^{(a)} \end{pmatrix}. \tag{6}$$

Replacing (5) with (6), we obtain the following relationship:

$$x^{(d)} = x_m^{(a)} - \frac{y_m^{(a)} \left(x_m^{(a)} - x_v^{(a)} \right) \sin\psi}{z_v^{(a)} \cos\psi + \left(y_m^{(a)} - y_v^{(a)} \right) \sin\psi} \tag{7}$$

$$y^{(d)} = \frac{z_v^{(a)} y_m^{(a)}}{z_v^{(a)} \cos\psi + \left(y_m^{(a)} - y_v^{(a)} \right) \sin\psi}. \tag{8}$$

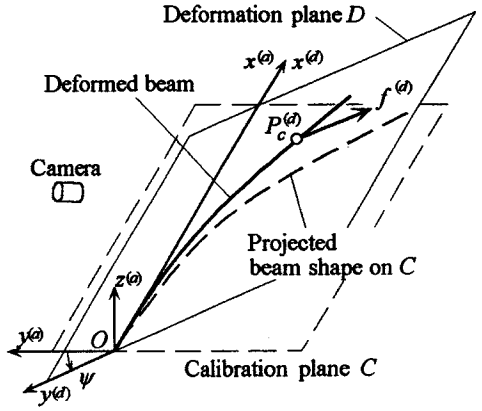

Fig. 4. Definition of the deformation plane.

C. Deformation of Antenna on C

We first note that the antenna under a contact force deforms in $\mathcal{D}$, as shown in Fig. 4. The antenna shape is given by the following equations on $\mathcal{D}$:

$$\text{Curved part } \left(0 \le x^{(d)} \le x_c^{(d)} \le L \right)$$

$$y^{(d)} = \frac{f^{(d)}}{6EI} \left(3x_c^{(d)} - x^{(d)} \right) \left\{ x^{(d)} \right\}^2 \tag{9}$$

$$\text{Linear part } \left(0 < x_c^{(d)} \le x^{(d)} \le L \right).$$

$$y^{(d)} = \frac{f^{(d)}}{6EI} \left(3x^{(d)} - x_c^{(d)} \right) \left\{ x_c^{(d)} \right\}^2 \tag{10}$$

where

$$f^{(d)} \equiv \sqrt{\left\{ f_y^{(a)} \right\}^2 + \left\{ f_z^{(a)} \right\}^2} \tag{11}$$

and $x_c^{(d)}$, L, E, and I denote the contact point, the total length of the antenna, Young's modulus of elasticity, and the second moment of area, respectively. Although (11) does not include the $f_x^{(a)}$ component, it should be small under a simple pushing motion to an object by a flexible beam. By considering this, we assume $f^{(d)} \approx \|\mathbf{f}^{(a)}\|$. In summary, (7) and (9)–(10) are a set of basic equations providing the contact information.

V. Solutions of Basic Equations

A. ψ Is Known

There are two cases where ψ is known. When a knife-edged object is placed perpendicular to the calibration plane $\mathcal{C}$, the deformation plane $\mathcal{D}$ coincides with $\mathcal{C}$. This holds $\psi = 0$. The other case is expected for the beam whose elasticity is not uniform but limited in a particular direction. A flat scale such as that made by plastic is a good example of this kind of beam, which Assumption 5) excludes. For such a beam, the deformation plane $\mathcal{D}$ never changes, irrespective of the direction of contact force. Therefore, ψ is determined uniquely.

When ψ is known, we can easily compute $(x^{(d)}, y^{(d)})$ from the measured point $(x_m^{(a)}, y_m^{(a)})$ by utilizing (7) and (8). Let us assume that we get two points $(x_1^{(d)}, y_1^{(d)})$ and $(x_2^{(d)}, y_2^{(d)})$ through a visual sensor.

1) Two Points from the Curved Part: From (9), we can obtain the following two equations:

$$y_1^{(d)} = \frac{f^{(d)}}{6EI}\left(3x_c^{(d)} - x_1^{(d)}\right)\left\{x_1^{(d)}\right\}^2 \tag{12}$$

$$y_2^{(d)} = \frac{f^{(d)}}{6EI}\left(3x_c^{(d)} - x_2^{(d)}\right)\left\{x_2^{(d)}\right\}^2 \tag{13}$$

where $x_c^{(d)}$ should satisfy the condition of $0 < x_1^{(d)} < x_2^{(d)} \leq x_c^{(d)} \leq L$. From (12) and (13), we can easily derive the unique set of solutions in $0 < x_1^{(d)} < x_2^{(d)} \leq x_c^{(d)}$ as follows:

$$f^{(d)} = 6EI\frac{\left\{x_2^{(d)}\right\}^2 y_1 - \left\{x_1^{(d)}\right\}^2 y_2^{(d)}}{\left\{x_1^{(d)}\right\}^2\left\{x_2^{(d)}\right\}^2\left(x_2^{(d)} - x_1^{(d)}\right)} \tag{14}$$

$$x_c^{(d)} = \frac{\left\{x_1^{(d)}\right\}^3 y_2^{(d)} - \left\{x_2^{(d)}\right\}^3 y_1^{(d)}}{3\left(\left\{x_1^{(d)}\right\}^2 y_2^{(d)} - \left\{x_2^{(d)}\right\}^2 y_1^{(d)}\right)}. \tag{15}$$

Note that $x_2^{(d)} - x_1^{(d)} \neq 0, \{x_1^{(d)}\}^2 y_2^{(d)} - \{x_2^{(d)}\}^2 y_1^{(d)} \neq 0, x_1^{(d)} \neq 0, x_2^{(d)} \neq 0$ under $0 < x_1^{(d)} < x_2^{(d)} \leq x_c^{(d)}$.

2) Two Points from the Linear Part: In this case, we can obtain the following two equations:

$$y_1^{(d)} = \frac{f^{(d)}}{6EI}\left(3x_1^{(d)} - x_c^{(d)}\right)\left\{x_c^{(d)}\right\}^2 \tag{16}$$

$$y_2^{(d)} = \frac{f^{(d)}}{6EI}\left(3x_2^{(d)} - x_c^{(d)}\right)\left\{x_c^{(d)}\right\}^2 \tag{17}$$

where $x_c^{(d)}$ should satisfy the condition of $0 < x_c^{(d)} \leq x_1^{(d)} < x_2^{(d)} \leq L$. From (16) and (17), we can introduce the unique set of solutions in $0 < x_c^{(d)} \leq x_1^{(d)} < x_2^{(d)}$ as follows:

$$f^{(d)} = 2EI\frac{-\left(y_1^{(d)} - y_2^{(d)}\right)^3}{9\left(x_2^{(d)} - x_1^{(d)}\right)\left(x_1^{(d)} y_2^{(d)} - x_2^{(d)} y_1^{(d)}\right)} \tag{18}$$

$$x_c^{(d)} = \frac{3\left(x_1^{(d)} y_2^{(d)} - x_2^{(d)} y_1^{(d)}\right)}{y_2^{(d)} - y_1^{(d)}}. \tag{19}$$

Note that $x_2^{(d)} - x_1^{(d)} \neq 0, y_2^{(d)} - y_1^{(d)} \neq 0, x_1^{(d)} y_2^{(d)} - x_2^{(d)} y_1^{(d)} \neq 0$ under $0 < x_c^{(d)} \leq x_1^{(d)} < x_2^{(d)}$.

3) One from Each of the Curved and Linear Parts: Without loss of generality, we can assume $0 < x_1^{(d)} \leq x_c^{(d)} \leq x_2^{(d)}$ and $x_1^{(d)} \neq x_2^{(d)}$. In this case, (9) and (10) exist for each point. From these equations, we obtain

$$\begin{aligned} g_{cl}\left(x_c^{(d)}\right) &= y_1^{(d)}\left\{x_c^{(d)}\right\}^3 - 3x_2^{(d)} y_1^{(d)}\left\{x_c^{(d)}\right\}^2 \\ &\quad + 3\left\{x_1^{(d)}\right\}^2 y_2^{(d)} x_c^{(d)} - \left\{x_1^{(d)}\right\}^3 y_2^{(d)} \\ &= 0. \end{aligned} \tag{20}$$

Equation (20) is the cubic equation with respect to $x_c^{(d)}$. From (20), we can easily show (21) and (22) under $0 < x_1^{(d)} \leq x_c^{(d)} \leq x_2^{(d)}$, $x_1^{(d)} \neq x_2^{(d)}$, and $0 < f^{(d)}$

$$\lim_{x_c^{(d)} \to -\infty} g_{cl}\left(x_c^{(d)}\right) = -\infty \tag{21}$$

$$\lim_{x_c^{(d)} \to +\infty} g_{cl}\left(x_c^{(d)}\right) = +\infty. \tag{22}$$

Now, let us examine the sign of $g_{cl}(x_1^{(d)})$ and $g_{cl}(x_2^{(d)})$. $g_{cl}(x_1^{(d)})$ and $g_{cl}(x_2^{(d)})$ can be rearranged in the following forms:

$$\begin{aligned} g_{cl}\left(x_1^{(d)}\right) &= \frac{f^{(d)}}{6EI}\left(x_c^{(d)} - x_1^{(d)}\right)\left\{x_1^{(d)}\right\}^3\left\{\left(3x_2^{(d)} - x_1^{(d)}\right)\right. \\ &\quad \times \left(x_c^{(d)} - x_1^{(d)}\right) + x_c^{(d)}\left(x_2^{(d)} - x_1^{(d)}\right) \\ &\quad \left. + 2x_c^{(d)}\left(x_2^{(d)} - x_c^{(d)}\right)\right\} \end{aligned} \tag{23}$$

$$\begin{aligned} g_{cl}\left(x_2^{(d)}\right) &= -\frac{f^{(d)}}{6EI}\left\{x_1^{(d)}\right\}^2\left(x_2^{(d)} - x_c^{(d)}\right) \\ &\quad \times \left\{x_c^{(d)}\left(2x_2^{(d)} + x_c^{(d)}\right)\left(x_2^{(d)} - x_1^{(d)}\right)\right. \\ &\quad + 2x_c^{(d)} x_2^{(d)}\left(x_2^{(d)} - x_c^{(d)}\right) \\ &\quad \left. + 2\left\{x_2^{(d)}\right\}^2\left(x_c^{(d)} - x_1^{(d)}\right)\right\}. \end{aligned} \tag{24}$$

Under the condition of $0 < x_1^{(d)} \leq x_c^{(d)} \leq x_2^{(d)}$, $x_1^{(d)} \neq x_2^{(d)}$, and $0 < f^{(d)}$, we can show $g_{cl}(x_1^{(d)}) \geq 0$ and $g_{cl}(x_2^{(d)}) \leq 0$. Conditions (21), (22), $g_{cl}(x_1^{(d)}) \geq 0$, and $g_{cl}(x_2^{(d)}) \leq 0$ ensure that we always have one solution between $x_1^{(d)}$ and $x_2^{(d)}$, while there are three solutions over the whole range.

Thus, the uniqueness of solution is guaranteed for Section V-A1 through V-A3 under Assumption 6). Now, a question that comes up is how the proposed system can determine whether the point is in the curved part or the linear part of the beam. For two points detected, we compute three candidates for the contact point by using the formula (Section V-A1 through V-A3). Then, we examine whether each candidate can satisfy each constraint condition, such as $0 < x_1^{(d)} < x_2^{(d)} \leq x_c^{(d)}$. The former discussions ensure that if one candidate satisfies its constraint condition, two others cannot. This is the basic way for computing the contact point. Of course, since visual data include some noise, we may have more than one solution satisfying the constraint condition. Such undesirable data will bring an error when computing the contact point. By taking an appropriate averaging process, we can suppress its influence on the computation of contact point. We call this version 2D-VBAA, where the beam deforms on a given plane. Now, note that there is a failure mode where the uniqueness of solution is not guaranteed. For example, consider the case where the beam makes contact with the object whose surface is almost parallel to it, as shown in Fig. 5(a). For a small pushing angle, line contact will happen instead of point contact, as shown in Fig. 5(b). This is what we call a failure mode in the sense that the discussions given in Section V–A1 through V-A3 can no longer be applied. In this paper, we exclude such failure modes by Assumption 5).

B. ψ Is Unknown

Let $(x_i^{(d)}, y_i^{(d)})$ $(i = 1, 2, 3)$ be the measured points. For $(x_1^{(d)}, y_1^{(d)})$ and $(x_2^{(d)}, y_2^{(d)})$, we have the relationship given by

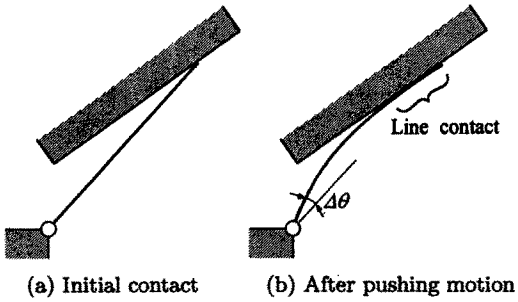

Fig. 5. A failure mode.

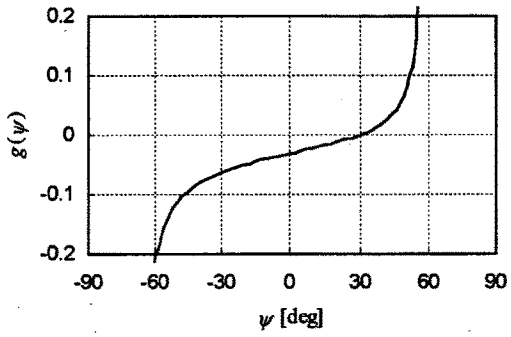

Fig. 6. A simulation result of the $g(\psi)$.

(15), and the same way for $(x_1^{(d)}, y_1^{(d)})$ and $(x_3^{(d)}, y_3^{(d)})$. Therefore, we can obtain

$$\frac{\left\{x_1^{(d)}\right\}^3 y_2^{(d)} - \left\{x_2^{(d)}\right\}^3 y_1^{(d)}}{\left\{x_1^{(d)}\right\}^2 y_2^{(d)} - \left\{x_2^{(d)}\right\}^2 y_1^{(d)}} = \frac{\left\{x_1^{(d)}\right\}^3 y_3^{(d)} - \left\{x_3^{(d)}\right\}^3 y_1^{(d)}}{\left\{x_1^{(d)}\right\}^2 y_3^{(d)} - \left\{x_3^{(d)}\right\}^2 y_1^{(d)}}. \tag{25}$$

We can regard that (25) is the nonlinear equation with respect to ψ, although it does not include ψ explicitly. For obtaining ψ numerically, we define $g_{3D}(\psi)$ as follows:

$$g_{3D}(\psi) = \frac{\left\{x_1^{(d)}\right\}^3 y_2^{(d)} - \left\{x_2^{(d)}\right\}^3 y_1^{(d)}}{\left\{x_1^{(d)}\right\}^2 y_2^{(d)} - \left\{x_2^{(d)}\right\}^2 y_1^{(d)}} - \frac{\left\{x_1^{(d)}\right\}^3 y_3^{(d)} - \left\{x_3^{(d)}\right\}^3 y_1^{(d)}}{\left\{x_1^{(d)}\right\}^2 y_3^{(d)} - \left\{x_3^{(d)}\right\}^2 y_1^{(d)}}. \tag{26}$$

For example, $g_{3D}(\psi)$ is given in Fig. 6, where $g_{3D}(\psi) = 0$ provides the solution of ψ. Once ψ is given, both $x_c^{(d)}$ and $f^{(d)}$ are automatically obtained. From Fig. 6, we can see the uniqueness of solution by means of numerical analysis, while we cannot prove it in a mathematical way. We call this version 3D-VBAA, where ψ is not given in advance.

C. An Extreme Case

While a general mathematical framework of 3D-VBAA is given in Section V-B, it is generally hard to solve the set of nonlinear equations, and a unique solution for contact information is guaranteed. To cope with this, we discuss a specific version of 3D-VBAA, where both a vision and a moment sensor are incorporated in the system, as shown in Fig. 7(a).

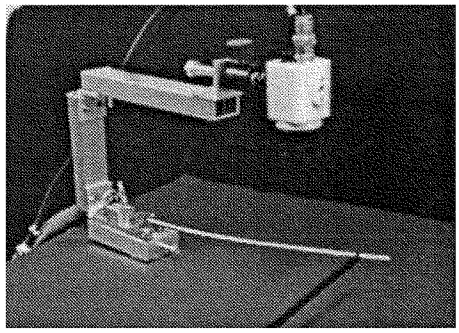

(a)

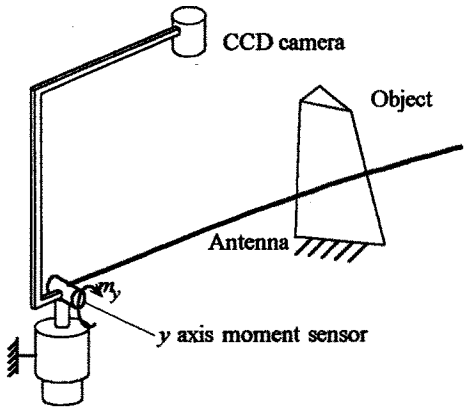

(b)

Fig. 7. (a) 2D-VBAA and (b) 3D-VBAA with a moment sensor.

The vision sensor is placed so that the visual axis may be perpendicular to the calibration plane and the distance between the plane and the sensor may be long enough. Under such a sensor arrangement, we can consider that the deformation plane coincides with the calibration plane. Since we can remove ψ from the unknown parameters, the problem finally results in two dimension. From the discussion of 2D-VBAA, we can obtain both the component of contact position $(x^{(a)}, y^{(a)})$ and the component of contact force $f_y^{(a)}$. The $z^{(a)}$ directional force component can be evaluated by the moment sensor output. Since $m_y = x_c^{(a)} f_z^{(a)}$

$$f_z^{(a)} = \frac{m_y}{x_c^{(a)}}. \tag{27}$$

By utilizing $f_y^{(a)}$ and $f_z^{(a)}$, we can estimate the beam displacement at the contact point as follows:

$$y_c^{(a)} = \frac{f_y^{(a)} \left\{x_c^{(a)}\right\}^3}{3EI} \tag{28}$$

$$z_c^{(a)} = \frac{f_z^{(a)} \left\{x_c^{(a)}\right\}^3}{3EI} \tag{29}$$

where $y_c^{(a)}$ and $z_c^{(a)}$ denote the beam displacements after it makes contact with the object. By estimating $y_c^{(a)}$ and $z_c^{(a)}$, we

can obtain the current contact point, which may differ from the initial one.

VI. Experimental Verification

We used the experimental setup shown in Fig. 7. The image data are fed into the computer through a CCD camera with 512 × 512 dots and 8 bits grayscale. For easily distinguishing the beam from the object, we use a white stainless beam with a diameter of 0.8 mm and a length of 240 mm. The deflections in the experiments are changed from approximately 5% (12 mm) up to 20% (48 mm) of the beam length. Therefore, the experiments partly include the results where Assumption 1) (linearity) is not always ensured. We believe that one of the big advantages of VBAA is that we can paint the beam so that it may be easily distinguished from the object. In order to suppress the frictional effect, we use an extremely slippery object.

A. 2D-VBAA

Fig. 7(a) shows an overview of the experimental system where we move the object instead of rotating both the camera and the moment sensor. In this experiment, the output from the moment sensor is not utilized. Now, recall that the contact point for the 2D-VBAA can be obtained by observing two arbitrary points on the beam. However, if we compute the contact point by using two points only, it may include a large error due to the digitizing error. In order to suppress such an error, we take an averaging process for the computed contact points by using more than 500 data. Fig. 8 shows the experimental results, where (a) and (b) show the estimated contact distance and the contact force, respectively, and $\Delta\theta$ denotes the pushing angle after making contact. The real lines and circles show the theoretical analysis and the experimental data, respectively. The agreement between analysis and experiments is fairly good.

The accuracy of the VBAA strongly depends on the thickness of the beam, the viewing area, and the resolution of the captured picture. Through experiments, it is found that the best accuracy is obtained when the camera captured the tip of the beam. This is probably because the tip of the beam shifts more than the base part. Under the best case, we succeed in detecting the contact point with the accuracy of ±2%.

B. 3D-VBAA with a Moment Sensor

Fig. 7(b) shows an overview of the experimental system, where a knife-edge-like object is used. Fig. 9(a) and (b) show experimental results, where (a) and (b) are the estimated contact distance and the direction of the estimated contact force respectively, and ν denotes the normal direction of the object surface. For this experiment, three objects with differing normal direction are used. As shown in Fig. 9(a), the estimation of contact distance can be executed with pretty high accuracy, even though the contact points do not exist on C. It can be seen from Fig. 9(b) that the estimated direction of contact force almost coincides with that of the normal direction of an object's surface. This is because the frictional effect is reduced as much as possible in the experiment.

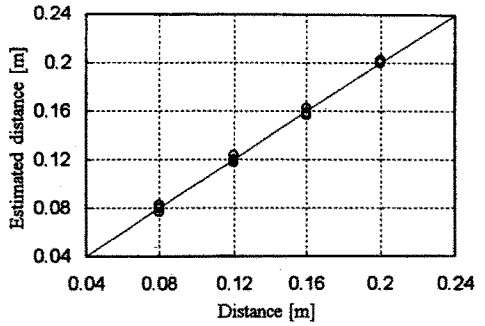

(a)

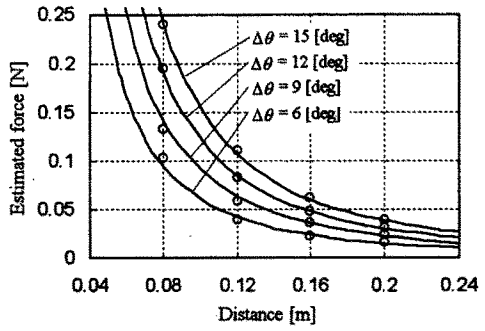

(b)

Fig. 8. Experimental results for 2D-VBAA.

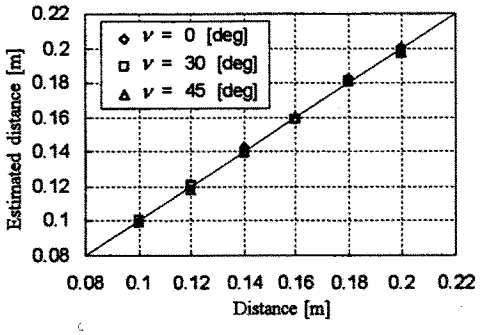

(a)

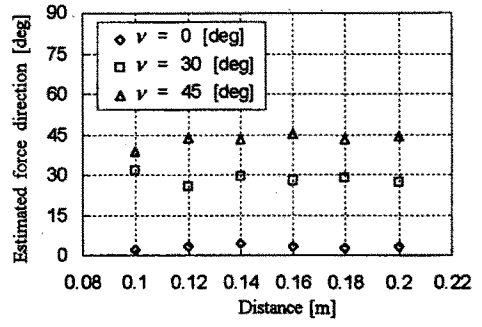

(a)

Fig. 9. Experimental results for 3D-VBAA.

C. Stiffness Sensing

Since the VBAA can estimate both the contact distance and the contact force continuously, it can evaluate the object's stiffness as well. If the object is very stiff, the contact point on the object does not move with respect to the absolute coordinate

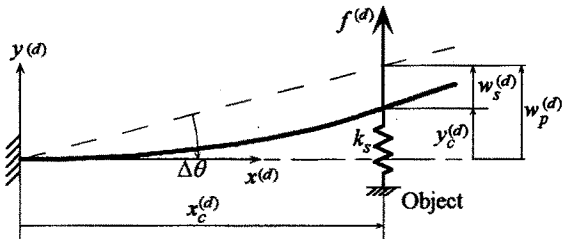

Fig. 10. Stiffness sensing by the VBAA.

system. This can be judged by examining the following condition:

$$w_s^{(d)} = w_p^{(d)} - y_c^{(d)} \tag{30}$$

where $w_s^{(d)}$ is the estimated shift of the contact point with respect to the absolute coordinate system and $w_p^{(d)} \approx x_c^{(d)}\Delta\theta$ is the virtual shift of the contact point on the beam assuming that there is no object, where $\Delta\theta$ is the pushing angle, as shown in Fig. 10. For $w_s^{(d)} \neq 0$, the object is judged to be compliant, while for $w_s^{(d)} = 0$, it has an extremely high stiffness. Now, suppose $f^{(d)}$ and $x_c^{(d)}$ are the estimated contact force and contact distance, respectively. For $w_s^{(d)} \neq 0$, we can evaluate the stiffness by

$$\hat{k}_s = \frac{f^{(d)}}{w_s^{(d)}} = \frac{f^{(d)}}{w_p^{(d)} - y_c^{(d)}}. \tag{31}$$

Note that the stiffness sensing does not make any influence on the contact point sensing and the contact force sensing, and it is independently evaluated after $f^{(d)}$ and $x_c^{(d)}$ are estimated.

Fig. 11 shows the experimental results for a compliant object, where (a)–(c) are the estimated contact distance, the estimated contact force, and the estimated stiffness, respectively. While most compliant objects include a highly nonlinear relationship between contact force and displacement, we utilize a tiny spring-based force measure so that we can keep a linear relationship between them. Fig. 11(b) tells us that we need an appropriate pushing angle ($\Delta\theta \geq 5$ [deg]), so that we can clearly estimate the contact force from the visual data. For the remaining data, except for $\Delta\theta = 3$ [deg], we should note that the estimated contact forces exist away from the lines expected by the analysis when a contact happens close to the base, while they are close to each other as the distance increases. There are a couple of reasons to explain such results. The first remark is that the equivalent stiffness of the beam drastically decreases with the increase of contact distance. This means that the total stiffness produced by both the beam and the object converges to that of the beam when a contact happens close to the beam, while it almost coincides with the object's stiffness when a contact occurs especially close to the base. The nice correlation between experimental data and analysis in the distance of approximately more than $x_c = 0.14$ [m] can be explained by reasoning that the stiffness model of the flexible beam is quite accurate. On the other hand, the part close to the base is mainly dominated by the object's stiffness, since the beam stiffness relatively increases at a point close to the base. When we utilize a spring-based force

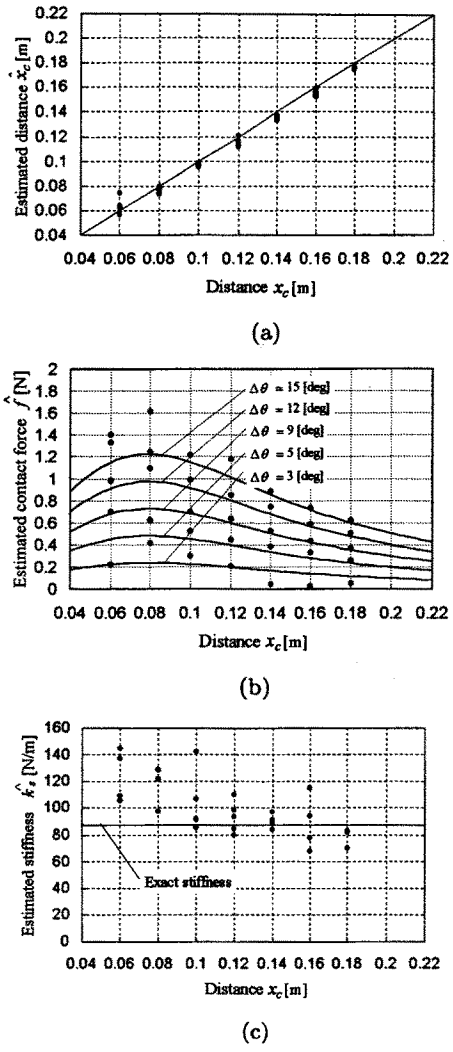

Fig. 11. Experimental results for a compliant object.

measure in a horizontal plane, there appears a direct contact between the spring part and the side cylinder. The friction caused by such a direct contact may bring a shift in the object's stiffness from the exact one according to each test. This means that the analytical line itself close to the base includes some ambiguity, since it is hard to input the exact object's stiffness under the use in horizontal plane. As shown in Fig. 11(c), the stiffness estimation is also not good when the contact happens particularly close to the base. The stiffness computation given in (31) requires $w_s^{(d)} = w_p^{(d)} - y_c^{(d)}$. When a contact happens at a point close to the base, $w_s^{(d)}$ becomes extremely small. Therefore, since $\hat{k}_s$ is computed by $f^{(d)}/w_s^{(d)}$, even a small error of $w_s^{(d)}$ leads to a large sensing error in the evaluation of the object's stiffness.

D. Influence of Occlusion

When using vision, we have to be very careful with both occlusion and lighting problems. The problem concerning occlusion will often appear when the object is compliant and the beam sinks into it during a pushing motion. Since the CCD camera takes a scene from the top view, the exact contact point on the beam and its neighborhood will often be hidden. The VBAA can overcome such an undesirable situation since it does not

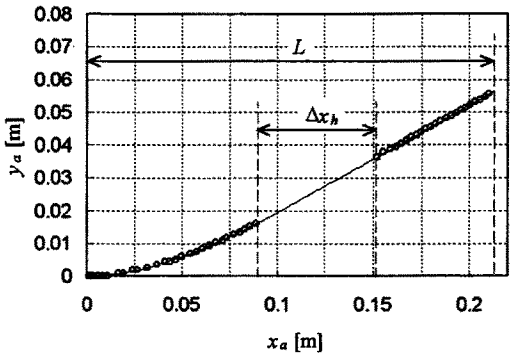

Fig. 12. An example of data with occlusion.

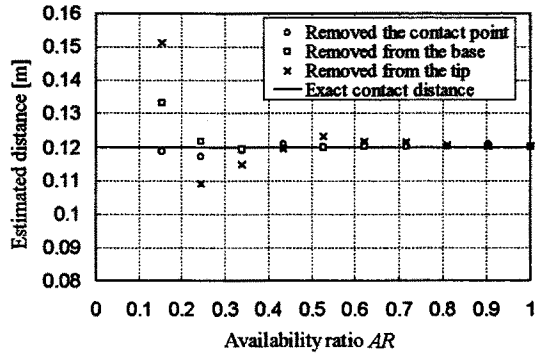

Fig. 13. The effect of occlusion on the sensing error.

need the exact contact point. Two arbitrary points on the beam can theoretically determine the full shape of the beam for a 2D-VBAA and, as a result, provide the contact force as well as the contact point. The contact force is estimated by utilizing the force-deformation relationship, while the contact point is evaluated from the geometrical relationship alone.

In order to evaluate the effect of occlusion, we purposely omit the measured data, as shown in Fig. 12, where Δx_h denotes the x_a directional distance in which the data on the beam are removed. Fig. 13 shows various results when all data are not available, where the horizontal axis denotes the availability ratio AR, which is given by

$$\mathrm{AR} = \frac{L - \Delta x_h^{(d)}}{L} \tag{32}$$

where L is the $x^{(d)}$ component of the beam tip. Since the deformation in the $y^{(d)}$ direction is extremely small compared with the beam length, L is almost equal to the beam length in the straight line. Note that theoretically, the 2D-VBAA can compute the contact length and the contact force if two arbitrary points are given. Because of this fact, even when more than 65% of data are removed, sufficiently high sensing accuracy is maintained in every case. Another interesting tendency is that we can keep the accuracy relatively high when utilizing the data with the inclusion of the tip of the beam. This is because one pixel difference leads to a large error on the curve estimation for the contact point close to the base, while it does not for the contact point close to the tip.

VII. Discussions

One application for the VBAA might be to utilize it as a force sensor in micro systems. Manipulation of biological cells may

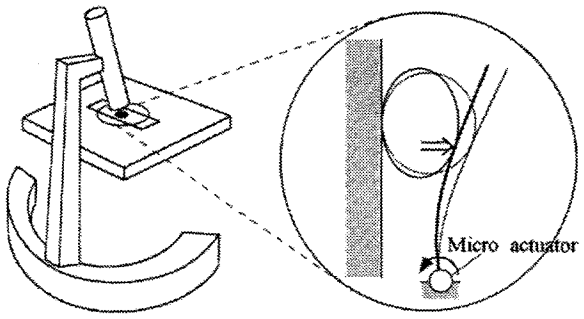

Fig. 14. An application example of VBAA.

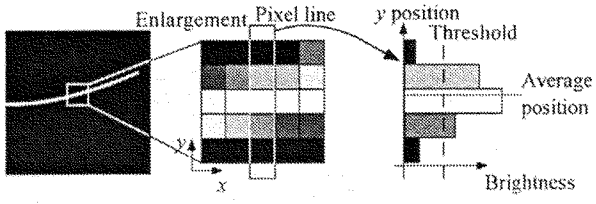

Fig. 15. Extracting the beam center from captured picture.

be a good example. Now, suppose that we measure the contact force between the cell and a micro manipulator. An object to be treated is extremely tiny, and therefore it is hard to implement any strain gauge into the system. Fig. 14 shows an example of such a manipulation system where a human can manipulate the object through the microscope and simultaneously the system can provide him or her with the manipulation force through either monitor or haptic sensation. Thus, the VBAA can be utilized as a kind of force observation system.

As for contact position, a vision sensor-based approach is generally lower in accuracy than a force sensor-based approach. This is because the force sensor has infinite resolution in principle, while the vision sensor is restricted by the number of pixels of CCD. Roughly speaking, the proposed VBAA has an accuracy of 2% in maximum, while the conventional force sensor-based approach maintains less than 1%.

Now, let us consider the way to increase the sensing accuracy. The image data are taken through a CCD camera and digitized into 512 × 512 dots. The computation of contact point depends on how the system chooses the representative point on the beam. We pick up the most likely point by taking an area-weighted averaging manner, as shown in Fig. 15. This approach is, of course, influenced by the lighting conditions. Therefore, the center of the beam may be determined more accurately by appropriately projecting an artificial light.

VIII. Conclusion

In this paper, we proposed a new sensing system vision-based active antenna that can detect the contact force, contact position, and stiffness of an object between a flexible beam and an object through the deformed flexible beam's shape. We introduce the basic equations for solving the contact point and the contact force. Even when the exact contact point is hidden by occlusion, the VBAA can still provide both the contact point and the contact force if two arbitrary points on the beam are observed for a 2D-VBAA or three points for a 3D-VBAA. While the vision

system generally requires much computing power for analyzing the images, this system does not. This is because it observes only the shape of a flexible beam. We also showed some experimental results to verify this idea.

REFERENCES

[1] G. Buttazzo, P. Dario, and R. Bajcsy, "Finger based explorations," in *Proc. SPIE Intelligent Robots and Computer Vision*, vol. 726, D. Casasent, Ed., 1986, pp. 338–345.

[2] S. Begej, "Planar and finger-shaped optical tactile sensors for robotic applications," *IEEE J. Robot. Automat.*, vol. 4, no. 5, pp. 472–484, 1988.

[3] M. R. Cutkosky and R. D. Howe, "Dynamic tactile sensing," presented at the Romansy'88: 7th CISM-IFToMM Symp. the Theory and Practice of Robots and Manipulators, Udine, Italy, 1988.

[4] D. Dornfeld and C. Handy, "Slip detection using acoustic emission signal analysis," in *Proc. IEEE Int. Conf. Robotics and Automations*, 1987, pp. 1868–1875.

[5] R. S. Fearing and T. O. Binford, "Using a cylindrical tactile sensor for determining curvature," in *Proc. IEEE Int. Conf. Robotics and Automations*, 1988, pp. 765–771.

[6] R. D. Howe, I. Kao, and M. R. Cutkosky, "The sliding of robot fingers under combined torsion and shear loading," in *Proc. IEEE Int. Conf. Robotics and Automations*, 1988, pp. 103–105.

[7] P. Dario and G. Buttazzo, "An anthropomorphic robot finger for investigating artificial tactile perception," *Int. J. Robot. Res.*, vol. 6, no. 3, pp. 25–48, 1987.

[8] D. L. Brock and S. Chiu, "Environment perception of an articulated robot hand using contact sensors," in *Proc. IEEE Int. Conf. Robotics and Automations*, 1987, pp. 89–96.

[9] H. Maekawa, K. Tanie, K. Komoriya, M. Kaneko, C. Horiguchi, and T. Sugawara, "Development of a finger-shaped tactile sensor and its evaluation by active touch," in *Proc. IEEE Int. Conf. Robotics and Automations*, 1992, p. 1327.

[10] R. A. Russell, "Closing the sensor-computer-robot control loop," *Robot. Age*, pp. 15–20, Apr. 1984.

[11] S. S. M. Wang and P. M. Will, "Sensors for computer controlled mechanical assembly," *Industrial Robot*, pp. 9–18, Mar. 1978.

[12] P. McKerrow, *Introduction to Robotics*. Reading, MA: Addison-Wesley, 1990.

[13] R. A. Brooks, "A robot that walks; emergent behaviors from a carefully evolved network," *Neural Computat.*, vol. 1, pp. 253–262, 1989.

[14] S. Hirose *et al.*, "Titan III: A quadruped walking vehicle," in *Proceedings of the Second International Symposium on Robotics Research*. Cambridge, MA: MIT Press, 1985.

[15] E. N. Schiebel, H. R. Busby, and K. J. Waldron, "Design of a mechanical proximity sensor," *Robotica*, vol. 4, pp. 221–227, 1986.

[16] R. A. Russell, "Using tactile whiskers to measure surface contours," in *Proc. 1992 IEEE Int. Conf. Robotics and Automation*, 1992, pp. 1295–1300.

[17] N. Ueno, M. M. Svinin, and M. Kaneko, "Dynamic contact sensing by flexible beam," *IEEE/ASME Trans. Mechatron.*, vol. 3, no. 4, pp. 254–264, 1998.

[18] S. A. Stansfield, "A robot perceptual system utilizing passive vision and active touch," *Int. J. Robot. Res.*, vol. 7, no. 6, pp. 138–161, 1988.

[19] P. K. Allen, "Integrating vision and touch for objects recognition tasks," *Int. J. Robot. Res.*, vol. 7, no. 6, pp. 15–33, 1988.

[20] D. Viscer, "Cooperating robot with visual and tactile skills," in *Proc. 1992 IEEE Int. Conf. Robotics and Automation*, 1992, pp. 2018–2023.

[21] S. Sakane, T. Ishikawa, and T. Sato, "Estimation of contact position between grasped object and environment based on sensor fusion of vision and force," *J. Robot. Soc. Jpn.*, p. 33, 1994. in Japanese.

[22] B. J. Nelson and P. K. Khosla, "Force and vision resolvability for assimilating disparate sensory feedback," *IEEE Trans. Robot. Automat.*, vol. 12, no. 5, pp. 714–731, 1996.

[23] M. Kaneko, "Active antenna," in *Proc. 1994 IEEE Int. Conf. Robotics and Automation*, 1994, pp. 2665–2671.

[24] M. Kaneko, N. Ueno, and T. Tsuji, "Active antenna (basic working principle)," in *Proc. 1994 IEEE Int. Conf. Intelligent Robotics and Systems*, 1994, pp. 1744–1750.

[25] M. Kaneko, N. Kanayama, and T. Tsuji, "3D active antenna for contact sensing," in *Proc. 1995 IEEE Int. Conf. Robotics and Automation*, 1995, pp. 1113–1118.

[26] ——, "Vision based active antenna," in *Proc. 1996 IEEE Int. Conf. Robotics and Automation*, 1996, pp. 2555–2560.

[27] N. Kanayama, M. Kaneko, and T. Tsuji, "Vision based active antenna—Basic considerations on two-points detecting method," in *Proc. 1996 IEEE/RSJ Int. Conf. Intelligent Robots and Systems*, 1996, pp. 444–449.

[28] ——, "On 3D vision based active antenna," in *Proc. 1997 IEEE Int. Conf. Robotics and Automation*, 1997, pp. 143–148.

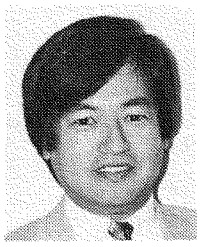

Makoto Kaneko (M'87–SM'00) received the B.S. degree in mechanical engineering from Kyushu Institute of Technology, Kitakyushu, Japan, in 1976 and the M.S. and Ph.D. degrees in mechanical engineering from Tokyo University, Tokyo, Japan, in 1978 and 1981, respectively.

From 1981 to 1990, he was a Researcher with the Mechanical Engineering Laboratory (MEL), Ministry of International Trade and Industry (MITI), Tsukuba Science City. From 1988 to 1989, he was a Postdoctoral Fellow at the Technical University of Darmstadt, Germany, where he joined a space robotics project. From 1990 to 1993, he was an Associate Professor of computer science and system engineering at Kyushu Institute of Technology. From November 1991 to January 1992, he was an Invited Professor at the Technical University of Darmstadt. Since 1993, he has been a Professor in the Industrial Engineering Department, Hiroshima University, Japan. His research interests include tactile-based active sensing, grasping strategy, legged locomotion sensor applications, and experimental robotics.

Prof. Kaneko was a Technical Editor of IEEE TRANSACTIONS ON ROBOTICS AND AUTOMATION during 1990–1994. He has been a Program Committee Member for the IEEE International Conference on Intelligent Robots and Systems since 1991. He was a Program Committee Member for the 1995, 1996, 1998, 1999, and 2000 IEEE International Conference on Robotics and Automation. He also was a Program Chairman for the 1998 International Conference on Advanced Mechatronics and a Program Cochairman for the 1999 IEEE International Conference on Intelligent Robots and Systems. He is a member of the IEEE Robotics and Automation Society, the IEEE Systems, Man, and Cybernetics Society, and the IEEE Industrial Electronics Society. He is also a member of Japan Society of Mechanical Engineers, Robotics Society of Japan, and Japanese Society of Instrumentation and Control Engineers.

Naoki Kanayama received the B.S. degree in mechanical system engineering from Kyushu Institute of technology, Iizuka, Japan, in 1994 and the M.S. and Dr.Eng. degree in information engineering from Hiroshima University, Hiroshima, Japan, in 1996 and 1999, respectively.

He is currently with Harmonic Drive Systems, Co., Ltd. His research interest is active sensing.

Dr. Kanayama received the Outstanding Young Engineering Award, Robotics Society of Japan, in 1994.

Toshio Tsuji (M'89) was born in Kyoto, Japan, on December 25, 1959. He received the B.E. degree in industrial engineering and the M.E. and Dr.Eng. degrees in system engineering from Hiroshima University, Hiroshima, Japan, in 1982, 1985, and 1989, respectively.

From 1985 to 1994, he was a Research Associate on the Faculty of Engineering, Hiroshima University. He was a Visiting Researcher at the University of Genoa, Italy, during 1992 to 1993. He is currently an Associate Professor in the Industrial Engineering Department, Hiroshima University. He has been interested in various aspects of motor control in robot and human movements. His current research interests focus on control in robot and human movements, control of EMG-controlled prostheses, motor control in human and robot movements, neural network, man–machine systems, and so forth.

Dr. Tsuji is a member of Japan Society of Mechanical Engineers, Robotics Society of Japan, and Japanese Society of Instrumentation and Control Engineers.